Jurnal Ilmu Fisika

Identification of Environmental Change in Bukit Kerang, Aceh Tamiang Regency Using Landsat Satellite Imagery

Sphinoza Lisnaria Simatupang[1], Rahmatsyah[1]

[1]Department of Physics, State University of Medan, Medan, Indonesia

Article Info	**ABSTRACT**
  Corresponding Author: Rahmatsyah Email: rahmatunimed@gmail.com	Changes in land cover and temperature in Bukit Kerang have been investigated using Landsat satellite images. We used Landsat 5 TM Landsat satellite imagery in 1988, Landsat 7 ETM in 2000, and Landsat 8 OLI in 2020. The ENVI 4.7 and ArcGIS 10.3 software was used to perform radiometric corrections, image cropping, image classification, image reclassification, calculating area, and layouts. Changes in land cover and land area in 1988, 2000, and 2020 affected the surface temperature conditions in those three years. In 1988, the dominant land area of forest cover was 5,926.44 ha (1 ha = 10^4 m^2), with the dominant temperature distribution of 17.2° C. In 2000, there was an increase in settlements by 25.56 ha and rice field area, which caused an increase in the temperature distribution of 19.7 – 25.4° C. In 2020, forest type land cover changes into plantations, fields, and settlements decreased by 3,731.91 ha, increasing temperature distribution of 20.6 – 21.8° C. Thus, there is a strong relationship between changes in land cover and change in surface temperature in Bukit Kerang area.

1. INTRODUCTION

Land cover is the physical features on earth surfaces that can be recognized by the distribution of vegetation, water, soil, and other manmade feature on the land as a result of human activities (Widyasamratri et al., 2019). This is caused by the habits of several regions where some people used to migrate out of town with economic factors as the main reason (Putri et al., 2019). Land cover is largely determined by the ecological conditions, altitudes, geological structure, and slope. Technological, socio-economic, and institutional setup influences the land-use pattern (Mishra et al., 2020). Geographic conditions and land use in a region also affect developing microclimate conditions, no matter the land-use factor or land cover of a region that is a little more to the surrounding air temperature, because it will influence the absorption of sunlight (Khafid, 2019). Land cover types have a vital role in protecting the environment from directly incurring incoming radiation and increasing the environment's aesthetical value. However, Land cover types have been changing over time and bringing rapid environmental modifications (Balew & Korme, 2020). Land cover has been changed to buildings, roads, and other impervious surfaces. The enormous changes with land cover lead to the urban heat island. The urban temperatures are 2-5 higher than those in rural surroundings (Jiang & Tian, 2010).

Remote sensing has become an essential tool for developing and understanding the global physical processes affecting the earth (Prasetya et al., 2019). In terms of land surface monitoring, the use of thermal remote sensing is very significant. Medium resolution of remote sensing data such as Landsat Thematic Mapper (TM), Enhanced Thematic Mapper Plus (ETM+), and Operational Land Imager (OLI)/ Thermal Infrared Sensor (TIRS) has been widely used in retrieving thermal information used for land surface temperature (LST) (Balew & Korme, 2020). The LST is the energy balance of land surface energy. The measurement of LST using satellite thermal infrared sensors from which brightness temperatures of land surfaces can be derived using Plank's law. LST is different for different surface properties thermal properties of land cover types. Each of these characteristics plays a wide range of variation with the land use and land cover change caused by the quick urbanization (Lv & Zhou, 2011).

This paper presents land cover change in Bukit Kerang, Bendahara, Aceh Tamiang. This area is one of the archaeological sites on Sumatra Island. There have been various studies for historical site areas, such as determining subsurface structures in the Sitopayan temple area (Nandari & Juliani, 2019), seawater intrusion rates in the Chinese City Site area (Rahmadani & Juliani, 2019), detection of subsurface archaeological sites at the Central Tapanuli Barus Kingdom archaeological site (Berutu et al., 2017), and earth magnet anomalies in Bahal Temple site – II in Portibi Village (Jernih & Rahmatsyah, 2019). Although there have been some studies around Bukit Kerang, research on land change is still limited. Indeed, the visual appearance shows that the land changes around Bukit Kerang have occurred significantly. This land change may threaten the existence of the archaeological sites in this area. Therefore, this study analyzes the land change in Bukit Kerang by utilizing the Landsat satellite data.

Figure 1 Research Location from Google Earth and USGS earth explorer.

2. METHOD

The research was conducted in the Bukit Kerang area (Figure 1). It is located at Mesjid Bdh, Bendahara, Aceh Tamiang Regency (03^0 53' – 04^0 32' N; 97^0 43' - 98^0 14' E).

Preprocessing process is a radiometric correction (to eliminate noise) on Landsat 8 OLI image, Landsat 7 ETM image, and Landsat 4 – 5 TM image. A radiometric correction is conducted from 1988, 2000, and 2020 image data, which is the stage of changing the pixel value (digital number) into a reflectance value. The pixel value (digital number) is first set to a radian value then converted to a reflectance value. The reflectance in the image uses ToA radiometric correction. Radiometric correction for all bands was performed using ENVI 4.7 software with equations for radiometric correction is ToA (Top of Atmosphere). The radiometric correction process in this study is obtained from calculating statistics which then displays the statistics on

the ArcGis 10.3 processing program. Image cutting using ArcGIS 10.3 software on Landsat 8 OLI imagery, Landsat 7 ETM imagery, and Landsat 4 – 5 TM path/row:129/57 imagery used with the administration limit Aceh Tamiang district. In guided classification techniques, users are involved in determining the sample area of each type of land use class, so the software will use the pixel values to recognize and group the areas within the scope of similar pixel values according to the desired class.

As a result of the radiometric correction, Landsat image cutting is then carried out in the classification stage using the Maximum Likelihood method. Classification techniques for imagery are supervised methods (based on digital image value) by making training areas obtained class grouping. Calculate NDVI is: Running ENVI 4.7, to search for NDVI, can be done in the transform menu and select NDVI. Input band 3 and band 4 on Landsat 5 TM and Landsat 7 ETM satellite imagery as band 4 and band 5 from Landsat 8 OLI imagery using NDVI equation, then perform information extraction. Calculating temperature: Running ENVI 4.7 to find the temperature value is done with the basic tool menu, then band math to enter the temperature formula to be added to the add list. The temperature value is converted into Celsius, and it must be reduced by -273 through the math band. NDVI processing used Equation 1 (Karismawati et al., 2019):

$$NDVI = \frac{NIR - Red}{NIR + Red} \tag{1}$$

where NIR is near infrared waves (0.63 µm - 0.69 µm), and red is red wave (0.76 µm - 0.90 µm).

Temperature processing (Temperature Index) was performed on satellite imagery of Landsat 5 TM, Landsat 7 ETM, and Landsat 8 OLI using the formula of TI utilizing band 6 (Long Wavelength Infrared) for Landsat 5 TM and Landsat 7 ETM at band 10 (Long Wavelength Infrared) on Landsat 8 OLI. To obtain the surface temperature value (temperature index) of Landsat imagery requires radiation correction with Qcal (DN value) 255 for Landsat 5 TM and Landsat 7 ETM, 65535 for Landsat 8 OLI, as well as constants Qmax, Qmin, Lmax, Lmin, contained in the metadata.

Processing temperature values used Equation 2 (Wiguna, 2017):

$$TI(K) = \frac{K_2}{L_n\left(\dfrac{K_1}{L_\lambda} + 1\right)} \tag{2}$$

where TI(K) is radian temperature (K), L_λ is spectral radian value, L_n is band 10 in radians, K_2 is absolute temperature calibration constant, K_1 is spectral radian calibration constant.

Image reclassification used ArcGIS software with the Input data from image classification to Arcgis software. The original image was compared with the results of land cover classification by editing the table attribute. After editing the image, save the table attribute. The imagery area is obtained using ArcGIS software, and ArcGIS software is also used for the layout.

3. RESULTS AND DISCUSSIONS

3.1 Radiometric Correction

The results of the radiometric correction make the pixel value of the satellite image better (Figure 2). The value corresponds to the meta data value. Each image has different conditions; it can be observed in the statistical image value before and after radiometric correction. Before the correction, the band value has a minimum value of 0, and a maximum value of band 1, band 3, band 4, band 5, band 6, and band 7 are 255. Band 2 has a max value is 206. After radiometric correction, the minimum value for ToA is -0.008290, and the minimum value is 0.634591 in band 1. Thus, there are statistical differences before and after radiometric correction for the minimum, maximum, mean, and standard deviation values, where DN results tend to be smaller after

correction. The results of the radiometric correction displayed on the image make the pixel value range of the satellite image narrower, as reported in a previous study (Utomo et al., 2017).

(Before)   (After)
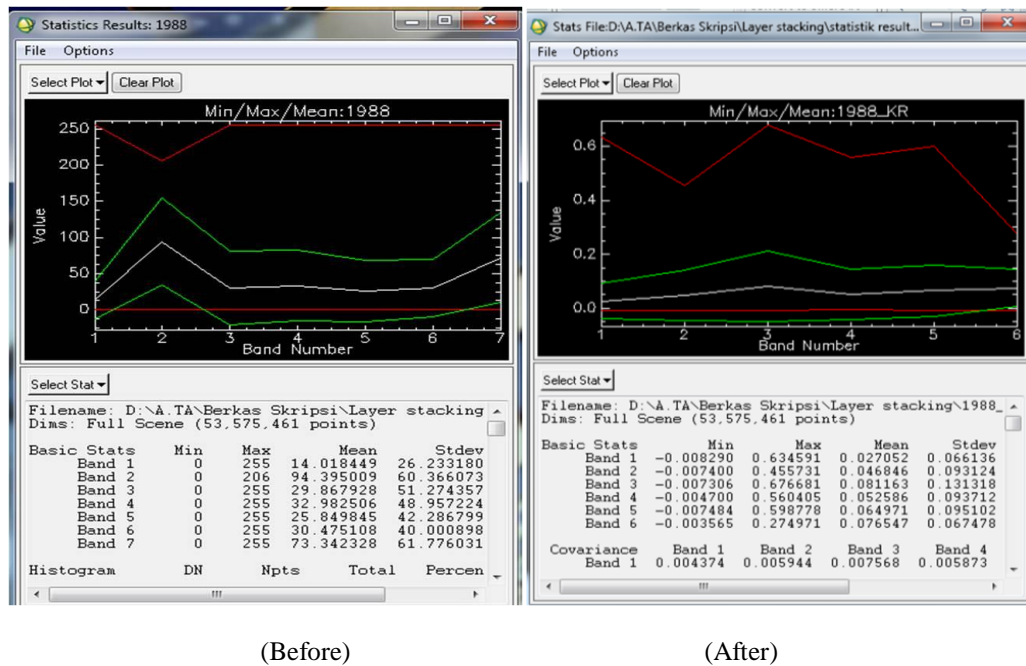
Figure 2 Radiometric Correction of Landsat Images

■ Research location for cropping
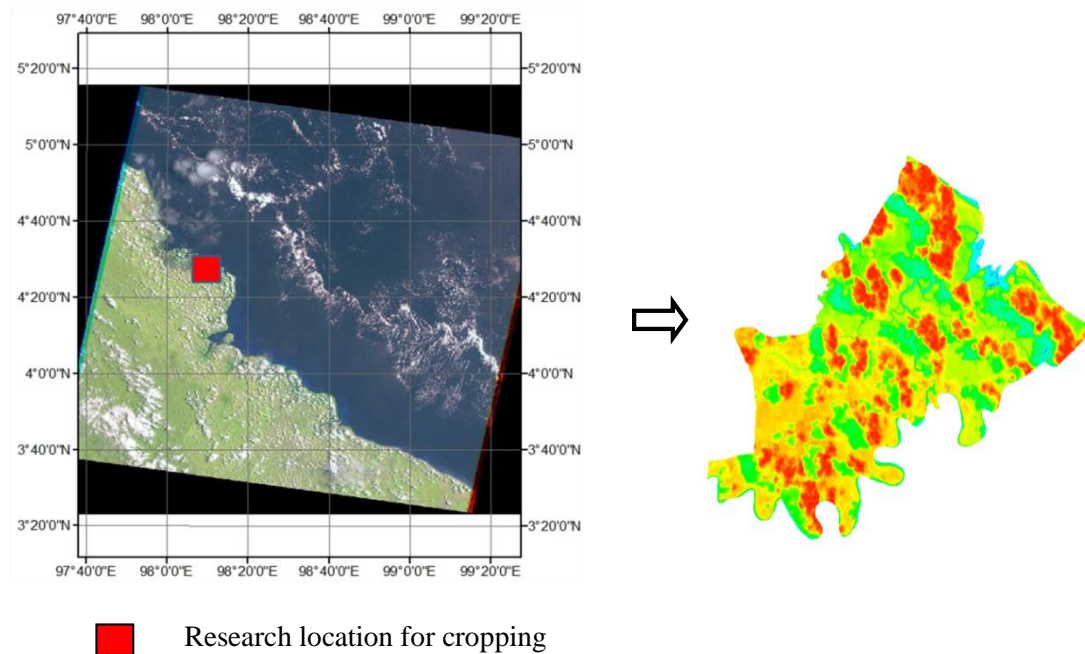
Figure 3 Image Cropping

3.2   Landsat Image Cropping

Cutting the Landsat image requires administrative boundaries in the form of vector data "Aceh Tamiang.shp" and satellite imagery from 1988, 2000, and 2020 compiled in raster format with a UTM coordinate function. : WGS 84, 47 N. The results of cutting satellite imagery of Landsat 5 TM, Landsat 7 ETM, and Landsat 8 OLI with the administrative boundaries of Aceh Tamiang can be seen in Figure 3.

3.3   Land Cover Type

Figure 4 provides an overview of the land cover map from Landsat 5 TM image in 1988, Landsat 7 ETM in 2000, and Landsat 8 OLI in 2020. Land cover types were determined based on class identifiers (signature class) obtained by creating a training area (Syam et al., 2012). In 1988, Landsat 5 TM imagery obtained four land cover indicators: rice fields, settlements, planters, and forests. Landsat 7 ETM image shows the four indicators of land cover obtained: rice fields, settlements, gardening, and forests, in 2000. Land cover types in 2020 are rice fields, settlements, planters, forests, and the field. The images' land cover types' appearance is displayed in different colors (Sampurno & Thoriq, 2016). The difference in land cover map results from Landsat image classification in 1988, 2000, 2020 can see on the dash – a break-up drew at five points shows a portion of forest land cover opened as plantation land. Vertical cross-section map of land cover in 1988, 2000, and 2020 as Figure 5.
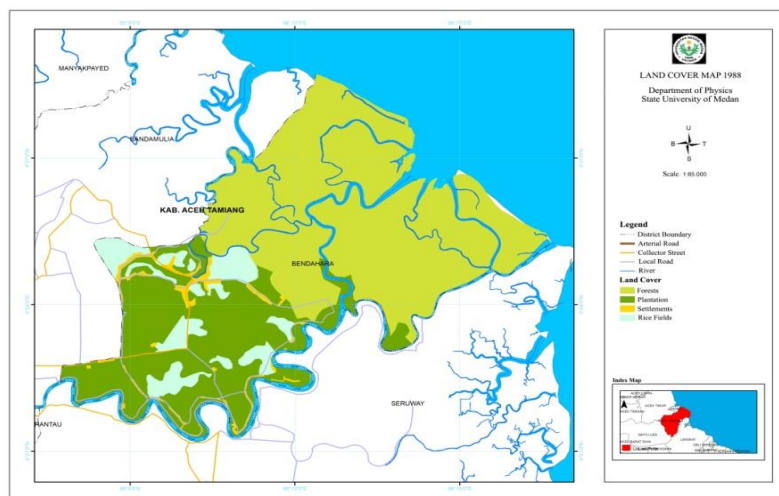
(a)
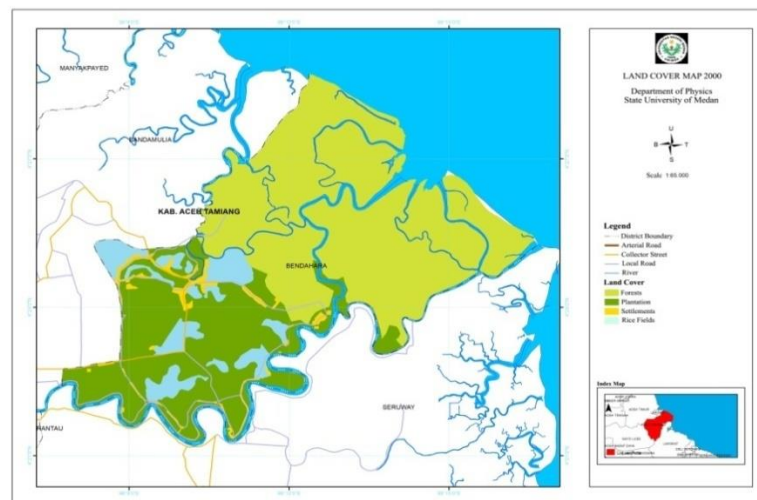
(b)

Figure 4 (a) Land cover in 1988 and (b) in 2000.
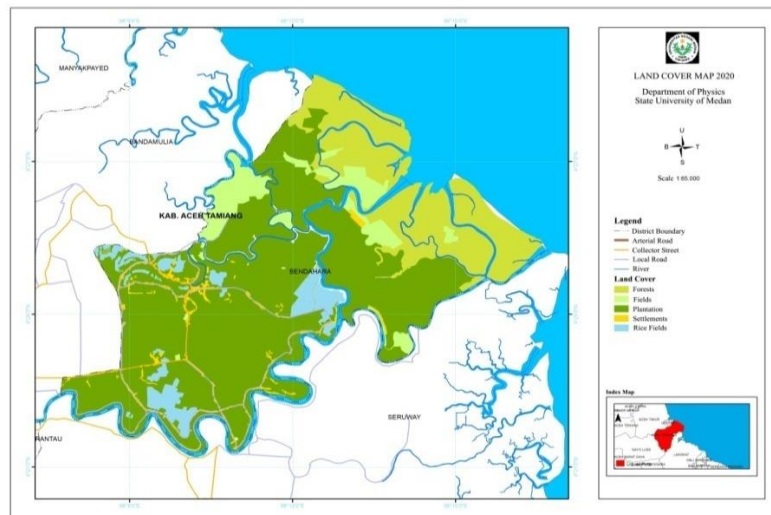
(c)

Figure 4 (continued) (c) land cover in 2020
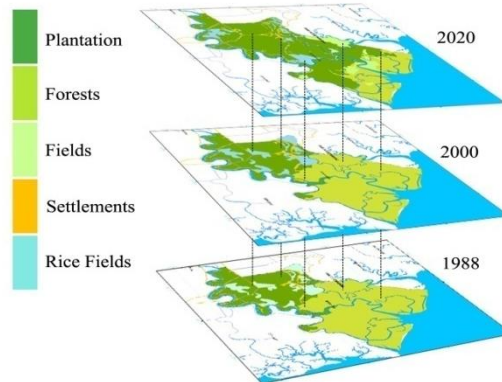
Figure 5 Vertical Cross-section map of Land Cover Differences

Table 1 shows the area change of classified land cover. In 1988, the rice fields area was 803.65 ha, settlements area was 242.90 ha, plantations area was 3,112.01 ha, and forests area was 5,926.44 ha. This number changed in 2000 in which rice fields are 804.67 ha, settlements area is 268.46 ha, plantations area is 3,099.42 ha, and forests area is 5,926.44 ha. In 2020, rice fields area becomes narrow, about 529.96 ha, settlements area is 273.89 ha, plantations area is 5,924.13 ha, forests area is 2180.53 ha, and fields area is 759.65 ha.

Table 1 Area Changes of Classified Land Cover.

Types of Land Cover	Area Land Cover (Ha)			Changes 1988 - 2000 (Ha)	Changes 2000 - 2020 (Ha)
	1988	**2000**	**2020**		
Rice Fields	803.65	804.67	529.97	1.02	-274.7
Settlements	242.90	268.46	273.89	25.56	5.43
Plantation	3,112.01	3,099.42	5,924.13	-12.59	2,822.71
Forests	5,926.44	5,912.44	2,180.53	-14.0	-3,731.91
Fields			759.65		759.65
Total	10,085	10,084.99	9,668.17	-0.01	-416.82

Changes in the land cover area of the Bukit Kerang are given in Table 1. The change in land cover from 1988 to 2000 was identified as rice fields with an increase of 1.02 ha. Since 1988, the number

of settlements has declined. An increase of 25.56 Ha in 2000 indicates that many residents were clearing rice fields as a means of livelihood. Meanwhile, land changes identified as plantations and forests experienced a reduction of 12.59 Ha and 14 Ha respectively from 1988 to 2000. In 2020, land cover classes experienced significant changes in plantations and forests. The plantations are mostly cleared with 2,822.71 Ha, which is consistent with reducing the 3,745.91 Ha forest area. The increasing number of residents causes the increase of land for livelihoods with an area of 759.65 Ha. The dominant type of plant in the Bendahara sub-district is the type of oil palm.

3.4 Surface Temperature

Change in land surface temperature form Landsat 5 TM, Landsat 7 ETM, and Landsat 8 OLI are given in Figure 6. Land surface temperature in 1988 was classified into five different classes with a range of surface temperature values from 17.2 C – 25.8 C. In 2000, the land surface temperature varied from 19.7 C – 25.4 C. Furthermore, Land surface temperature in 2020 varied from 12,1 ℃ – 25,4 ℃.

Changes in land cover resulted in a change in land surface temperature in the shell hill area, Treasurer, and Aceh Tamiang. The surface temperature has a higher value on the cover than the built-in land because, on the built-in land, there is no absorption of radiation, reflecting more so that there is accumulation in the air. The majority of temperature spread in the Bukit Kerang area, Bendahara, in 1988 was the temperature class 22,9℃ – 23,7℃ indicated by yellow class, and less for temperature class 25℃ – 25,8℃ (red class). The temperature distribution in 2000 was almost equal, but the occurrence of temperature class 23,3 ℃ – 25,4 ℃ (red) is minimal. The distribution of temperature in 2020 is dominated by the temperature class of 20,6 ℃ – 21,8 ℃ (orange) and the temperature class of 21,9 ℃ – 25,4 ℃ (red).

Change in temperature distribution is significant for 22.9 C – 23.7 C and 21.9 C – 25.4 C classes. This pattern is consistent with changes in land cover from forest areas to plantation areas, settlements, and fields. The increase in the growth of built-up land and the decrease in open land area in 2000 made the area with high surface temperature wider. On the other hand, an increase in temperature also occurred in 2020. About 3,731.91 Ha of forest land was converted into plantation land.
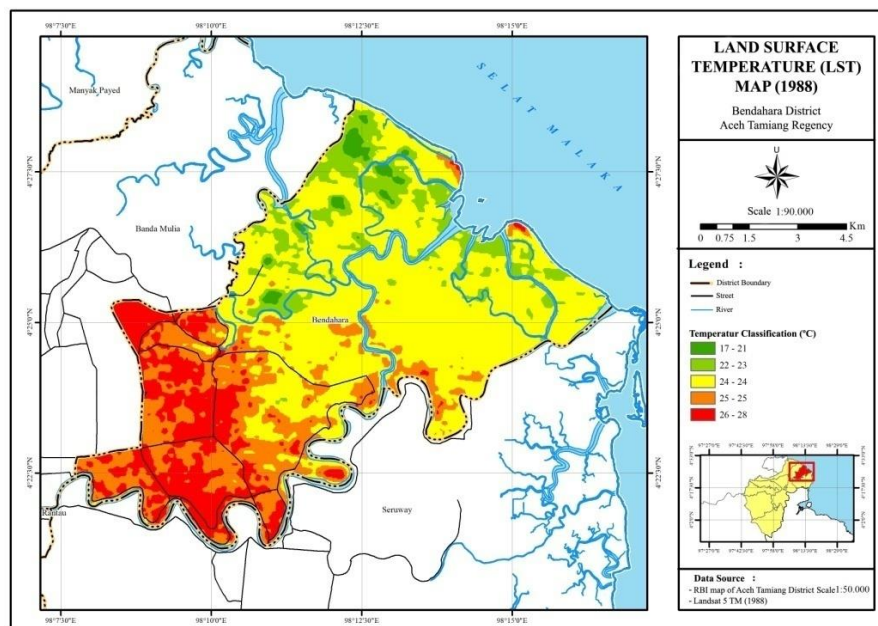
(a)

Figure 6 Surface temperature in 1988 (a)
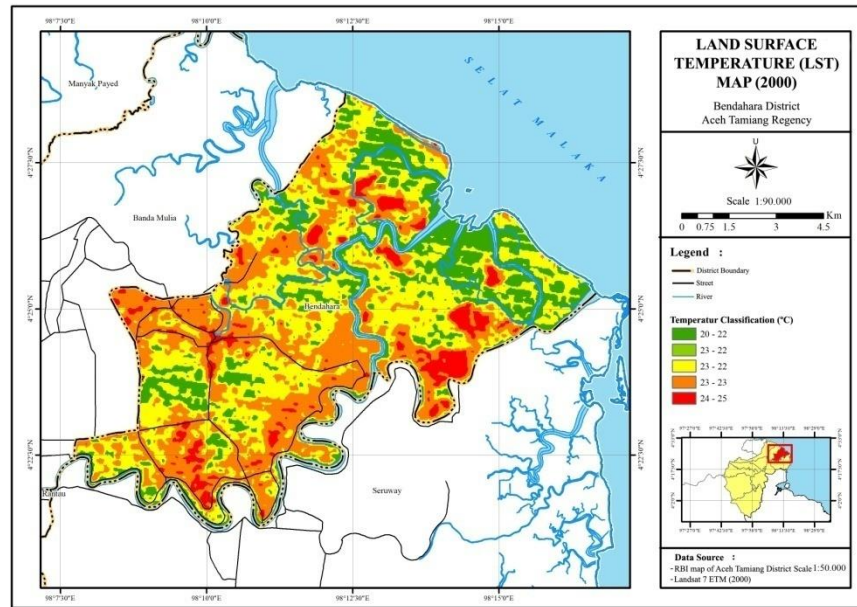
(b)
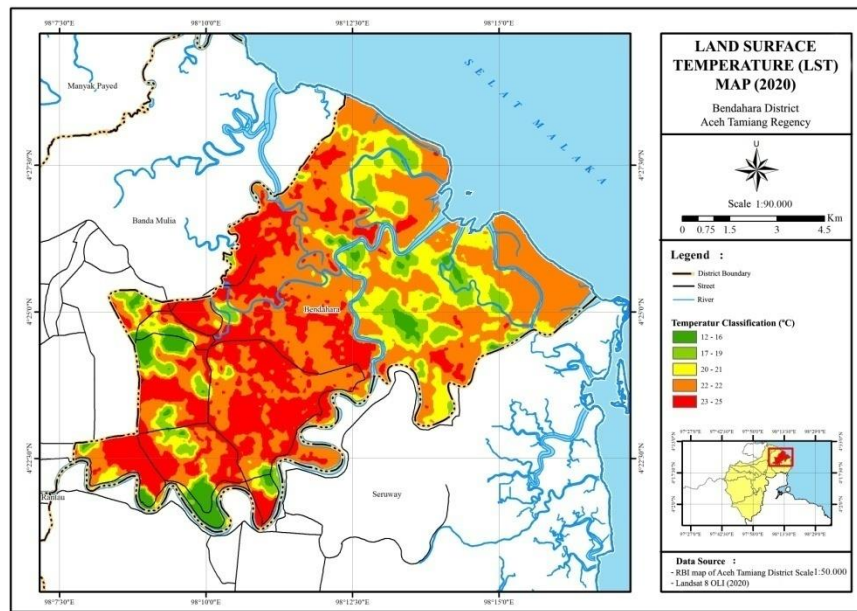
(c)

Figure 6 (continued) (b) surface temperature in 2000 and (c) in 2020.

4. CONCLUSION

Land cover change in Bukit Kerang was observed significantly. Between 1988 and 2000, there were four types of land cover, i.e., rice fields, settlements, plantations, and forests. In 2020, the land cover indicators became five types: rice fields, settlements, plantations, forests, and fields. Changes in the land cover area in 1988, 2000, and 2020 for rice fields are 803.65 ha, 804.67 ha, and 529.96 ha, respectively. For settlements, the change in areas is 242.90 ha, 268.46 ha, and 273, 89 ha. Plantations have 3,112.01 ha, 3,099.42 ha, 5,924.13 ha, forests have 5,926.44 ha, 5,926.44 ha, 2,180.53 ha, and in 2020 fields has areas of 759, 65 ha. Land cover change influences the surface temperature in Bukit

Kerang. In 1988, the surface temperature ranges were 17.2 C – 25.8 C and increased to 19.7 C – 25.4 C in 2000 and 12.1 C – 25.4 C in 2020.

REFERENCE

Balew, A., & Korme, T. (2020). Monitoring land surface temperature in Bahir Dar city and its surrounding using Landsat images. *Egyptian Journal of Remote Sensing and Space Science*, *23*(3), 371–386. https://doi.org/10.1016/j.ejrs.2020.02.001

Berutu, A., Hasibuan, J., Sakdiah, H., & Rahmatsyah. (2017). Study of Subsurface Early Detection of Archaeological Sites Based on Combination of Geoelectrical Methods with Geomagnetic Methods in Central Tapanuli. *Jurnal Geliga Sains: Jurnal Pendidikan Fisika*, *5*(1), 8. https://doi.org/10.31258/jgs.5.1.8-15

Jernih, H., & Rahmatsyah. (2019). The Existence Of The Bahal Ii Temple Site With Geomagnetic Methods. *EINSTEIN (E-Journal)*.

Jiang, J., & Tian, G. (2010). Analysis of the impact of Land use/Land cover change on Land Surface Temperature with Remote Sensing. *Procedia Environmental Sciences*, *2*(5), 571–575. https://doi.org/10.1016/j.proenv.2010.10.062

Karismawati, A., Sukmono, A., & Sasmito, B. (2019). Comparative Analysis of Dryness Identification of Rice Fields with Drought Index and Vegetation Index Methods on Landsat 8 Imagery (Case Study: Kendal Regency, Central Java). *Jurnal Geodesi Undip*, *8*(4), 21–30.

Khafid, M. A. (2019). Correlation analysis of the impact of land cover change and ratio vehicles on the dynamic of land surface temperature: Case studies of Cirebon City, Province of West Java. *IOP Conference Series: Earth and Environmental Science*, *399*(1). https://doi.org/10.1088/1755-1315/399/1/012096

Lv, Z. Q., & Zhou, Q. G. (2011). Utility of Landsat image in the study of land cover and land surface temperature change. *Procedia Environmental Sciences*, *10*(PART B), 1287–1292. https://doi.org/10.1016/j.proenv.2011.09.206

Mishra, P. K., Rai, A., & Rai, S. C. (2020). Land use and land cover change detection using geospatial techniques in the Sikkim Himalaya, India. *Egyptian Journal of Remote Sensing and Space Science*, *23*(2), 133–143. https://doi.org/10.1016/j.ejrs.2019.02.001

Nandari, C., & Juliani, R. (2019). Determination Of The Under Surface Structure Of The Sitopayan Temple Area. *EINSTEIN (E-Journal)*, 1–5.

Prasetya, T. A. E., Munawar, Taufik, M. R., Chesoh, S., Lim, A., & McNeil, D. (2019). Land Surface Temperatur Assessment in Central Sumatra, Indonesia. *Indonesian Journal of Geography*, *52*(2), 239–245. http://marefateadyan.nashriyat.ir/node/150

Putri, R. F., Budiman, L. S., Adalya, N. M., & Fauziyanti, N. U. (2019). Trend Analysis of Land Cover Changes, Population and Settlement Distribution to Land use Assessment in Kebumen Regency. *Jurnal Geografi*, *16*(1), 25–31. https://doi.org/10.15294/jg.v16i1.17749

Rahmadani, N., & Juliani, R. (2019). Determination Of Seawater Intrusion Level Using The Geoelectric Method Of Wenner Schlumberger Configuration And Conductivity Timeter Configuration In The China City Site Area. *EINSTEIN (E-Journal)*, 37–46.

Sampurno, R. M., & Thoriq, A. (2016). Land Cover Classification Using Landsat 8 Operational Land Imager (OLI) Images In Sumedang District. *Journal Teknotan*, *10*.

Syam, T., Darmawan, A., Banuwa, I. S., & Ningsih, K. (2012). Use Of Satellite Imagery In Identifying Land Cover Changes. *Globe*, *14*(2), 146–156.

Utomo, A. W., Suprayogi, A., & Sutomo, B. (2017). Analysis Of The Relation Between Land Surface Temperature Variations And Land Cover Classes Using Landsat Satellite Imagery Data (Case Study : Pati District). *Jurnal Geodesi Undip*, *6*(2), 71–80.

Widyasamratri, H., Souma, K., & Suetsugi, T. (2019). Study of urban temperature profiles on the various land cover in the Jakarta Metropolitan Area, Indonesia. *Indonesian Journal of Geography*, *51*(3), 357–363. https://doi.org/10.22146/ijg.45934

Wiguna, D. P. (2017). Identification of Soil Surface Temperature With Digital Number Conversion Method Using Remote Sensing Techniques And Geographic Information Systems. *Jurnal Teknologi Informasi Dan Komunikasi*, *6*(2), 59–69.